Semicond. Sci. Technol. **15** (2000) 189–196. Printed in the UK PII: S0268-1242(00)02390-7

Exciton dynamics and valence band mixing in tensile-strained semiconductor quantum wells

E Pérez†, L Viña†, E S Koteles‡, K M Lau§, A Di Carlo‖ and P Lugli‖

† Departamento de Física de Materiales, Universidad Autónoma de Madrid, Cantoblanco, E-28049 Madrid, Spain
‡ Institute for Microstructural Sciences, NCR, Ottawa K1A 0R6, Canada
§ Electrical and Computer Engineering Department, University of Massachusetts, Amherst, MA 01003, USA
‖ INFM-Dipartimento di Ingegneria Elettronica, Universitá di Roma, 'Tor Vergata', 00133 Roma, Italy

Received 5 March 1999, in final form 27 September 1999, accepted for publication 17 December 1999

Abstract. We have investigated the influence of the electronic band structure on the exciton dynamics in GaAsP tensile-strained quantum wells. We have found that the exciton cooling time is notably reduced when the heavy- and light-hole excitons are degenerate. The lifetime of the heavy-hole exciton is ∼300 ps whereas it is ∼500 ps for the light-hole exciton. Furthermore, we have determined, from the initial degree of polarization of the emission, the valence-band mixing as a function of the energy splitting between the heavy-hole and light-hole subbands. The degree of mixing is in qualitative agreement with tight-binding calculations.

1. Introduction

The electronic band structure around the fundamental gap in a III–V semiconductor quantum well (QW) can be conveniently tailored by means of a biaxial tensile strain. The effect of this is opposite to that of the confinement: while the latter increases the gap and raises the light-hole (lh) subband above the heavy-hole (hh) subband in the growth direction, the tensile strain decreases the gap and rises the hh subband above the lh one [1, 2]. Thus, the band structure of a tensile-strained QW is determined by the balance between the confinement and the tensile strain effects.

The optical excitation of a QW above the fundamental gap promotes electrons to the conduction band (CB) leaving holes in the valence band (VB). These electron–hole pairs rapidly form hot excitons in their ground and excited states [3]. The excitons lose kinetic energy to reach the states with $\boldsymbol{K} = \boldsymbol{0}$ of their ground state and recombine giving rise to luminescence. Selecting the well width, in order to fix the confinement degree, and the materials for the well and the barrier, in order to create tensile-strained QWs and thus to determine a strain degree, it is possible to create new subband structures and to obtain QWs whose excitonic ground state is of hh, lh or degenerate hh–lh character (in the following we shall denote hh and lh excitons as HH and LH, respectively). This is very interesting from the fundamental and technological point of view. The coincidence of HH and LH causes an increment in the absorption coefficient at the energy of the gap, which could enhance the efficiency of photodiodes and high-velocity optical modulators [4, 5]. Systems whose lowest valence subband is of lh character are appropriate for low-threshold-current lasers, due to their lower density of states, and for high-mobility transistors, as mobility is inversely proportional to the carrier effective mass [2].

In this paper we present a study of the exciton dynamics and valence band mixing (VBM) as a function of the electronic band structure in six different GaAsP tensile-strained QWs. We will show that the density of states and the effective mass of the excitonic ground state modify the characteristic times of the exciton dynamics. An analysis of the initial degree of polarization of the emission indicates that the degree of VBM depends strongly on the energy splitting between the hh and lh subbands. This could have important consequences on the spin relaxation time of holes since the VBM is the main mechanism responsible for their spin flip [6].

2. Experimental details and sample characterization

We have investigated six different $GaAs_{1-x}P_x$ QWs with well widths of 80 and 120 Å and phosphorus compositions

Table 1. Energy splitting between the hh and lh subbands (Δ) at the centre of the zone, Stokes shift (SS), hh (E_{b-hh}) and lh (E_{b-lh}) exciton binding energies and heavy-hole (m^*_{hh}) and light-hole (m^*_{lh}) effective masses in the well plane, for the six $GaAs_{1-x}P_x$ QWs whose well widths are 80 Å and 120 Å and whose phosphorus compositions are 5%, 8% and 12% (data taken after [9]).

P (%)	Δ (meV)	SS (meV)	E_{b-hh} (meV)	E_{b-lh} (meV)	m^*_{hh} (m_0)	m^*_{lh} (m_0)
80 Å QWs						
5	16.5	8	11.3	18.6	0.17	0.11
8	−0.9	10	12.5	14.2	0.29	−0.38
12	3.2	17	10.3	20	0.23	−1
120 Å QWs						
5	−0.7	9	7.7	9.8	−1.25	−0.29
8	−12.4	7	8	10	0.40	0.66
12	−16.9	8	8	9	0.24	0.28

(x) of 5%, 8% and 12%. The wells were separated by 400 Å $Ga_{0.65}Al_{0.35}As$ barriers. The samples were grown by metal organic chemical vapour deposition on GaAs(100) substrates, 2° oriented towards the (110) direction [7]. As the lattice parameter of the $GaAs_{1-x}P_x$ QWs is smaller than that of the $Ga_{0.65}Al_{0.35}As$ barriers, the wells grow under biaxial tensile strain in the perpendicular plane to the growth direction; the degree of strain depends on the phosphorus composition. Since the band structure is determined by the balance between the confinement and strain effects, the lowest valence band, and therefore the excitonic ground state, can be of hh, lh or degenerate hh–lh character. The latter case occurs when the confinement effect compensates the strain effect. It is important to notice that the relative positions of the HH and LH do not need to be the same as the relative positions of the hh and lh subbands, because the binding energy of the HH and LH are, in general, different.

We have employed time-resolved photoluminescence spectroscopy to study the dynamic behaviour of the systems. The samples were optically excited with pulses from a Styryl 8 or Pyridine 1 dye-laser synchronously pumped by a mode-locked Nd-YAG laser. The photoluminescence (PL) was time resolved by means of an up-conversion spectrometer with a time resolution of ∼5 ps. For the analysis of the VBM, the exciting light was σ^+ circularly polarized and the PL was analysed into its σ^+ and σ^- components in order to obtain the degree of polarization of the luminescence, defined as $\boldsymbol{P} = (I^+ - I^-)/(I^+ + I^-)$, where $I^+(I^-)$ is the intensity of the $\sigma^+(\sigma^-)$ polarized light. Unless stated otherwise the experiments were performed at 5 K.

The band structure of these $GaAs_{1-x}P_x$ QWs has been analysed in the past [7–9]. Bertolet *et al* [7] determined the energy positions of the excitonic peaks by photoluminescence excitation spectroscopy (PLE). Viña *et al* [9] studied the exciton binding energy and the dispersion relation of the hh and lh subbands by PLE measurements in the presence of a magnetic field applied in the Faraday configuration. Figure 1 shows the PLE spectra of the six QWs. The measurements were made exciting with σ^+ polarized light and detecting the σ^- emission, in order to establish the heavy/light character of the excitons: the low- (high-) intensity peaks correspond to the LH (HH) excitons. The spectra with only one structure depict the degenerate case, where the HH and LH excitons coincide in energy. The (80 Å, 5%) QW [10] shows a 'normal' structure with HH being the ground state. The (120 Å, 8%) and (120 Å, 12%) QWs present an 'inverse' configuration, where the ground state is the LH exciton and

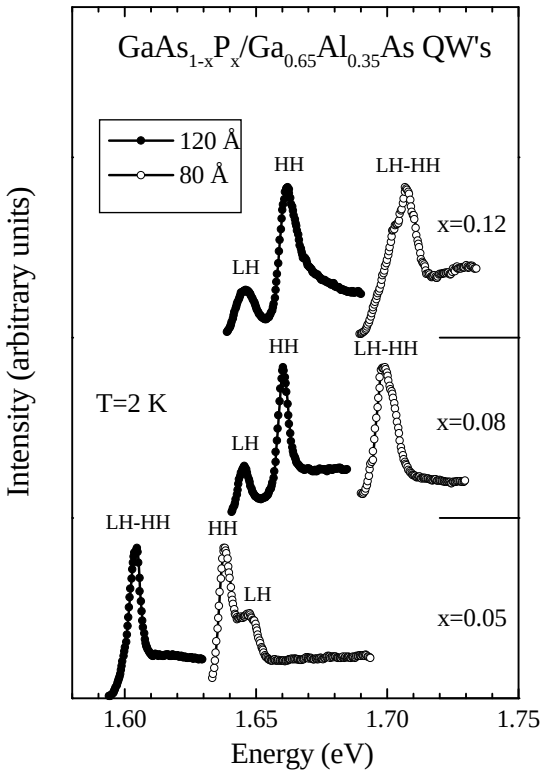

Figure 1. Photoluminescence excitation spectra, PLE, of the six $GaAs_{1-x}P_x$ QWs. The solid (open) points correspond to the 120 Å (80 Å) QWs. The spectra were taken at 2 K, exciting with σ^+ polarized light and detecting the σ^- polarized light. (After [9]).

the other three QWs correspond to the degenerate case, in which HH and LH appear at the same energy.

Table 1 compiles the most important properties necessary to analyse the dynamic behaviour of each QW. The table includes the energy splitting between the hh and lh subbands at the centre of the zone ($\Delta = E_{hh} - E_{lh}$), the Stokes shift (SS), the HH (E_{b-hh}) and LH (E_{b-lh}) binding energies and the in-plane hh (m^*_{hh}) and lh (m^*_{lh}) effective masses. A positive Δ means that the lh subband has a higher energy than the hh one and therefore a 'normal' structure. The order of the hh and lh subbands is the same as that of HH and LH for all the wells except for the (80 Å, 12%) QW, in which Δ is positive but LH is slightly below HH, as can be appreciated by the presence of a weak shoulder in figure 1. The excitons in our system are localized, as can be easily concluded from the cw characterization: the Stokes shifts,

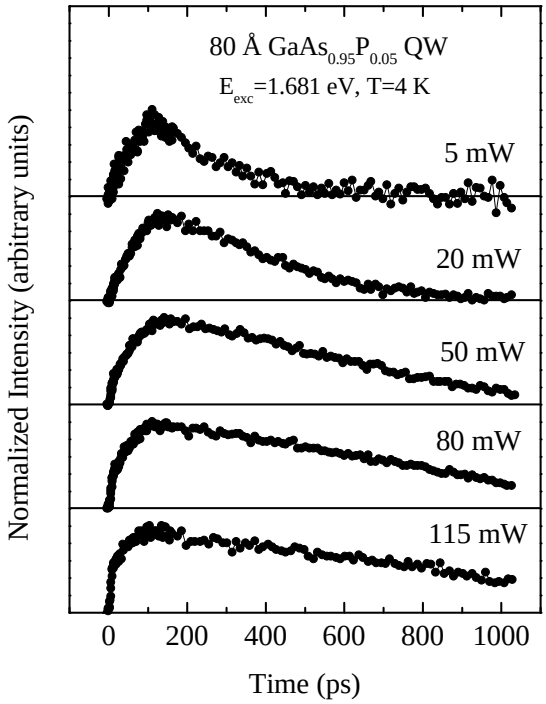

Figure 2. Time evolutions of the PL emitted by the 80 Å $GaAs_{0.95}P_{0.05}$ QW taken at different excitation powers. The temperature was fixed to 4 K and the excitation energy to 1.681 eV.

shown in table 1, are far from negligible, indicating that deep potential minima exist in the QWs [11]; furthermore, the widths of the emission spectra (∼9 meV) are much larger than typical excitonic homogeneous widths [12].

3. Results and discussion

3.1. Exciton dynamics

The main stages of the carrier dynamics in intrinsic QWs have been established in the past [13]. First of all, the photoexcited electron–hole pairs form hot excitons in their ground and excited states in ∼10 ps. The excitons interact rapidly among themselves and attain a thermalized distribution; the initial T of the thermal distribution is higher than that of the lattice. The excitons cool and reach the lattice T in ∼100 ps by scattering with phonons. The 'cold' excitons live hundreds of picoseconds before recombining either radiatively or non-radiatively. Our $GaAs_{1-x}P_x$ QWs constitute an unique system to study the influence of the band structure on the characteristic times and processes involved in the exciton dynamics.

Let us start by presenting the results of varying the photoexcited carrier density on the excitonic dynamics. As shown in figure 2, two different effects are observed with increasing power. In first place, the PL decay time increases. Secondly, two different PL rise times become discernible; one of them is of the order of ∼100 ps. The second one, whose importance increases with excitation power, is comparable to our time resolution, 5 ps. In the simplest analysis of the temporal evolution of the PL the rise, τ_{rise}, and decay, τ_{dec}, times are used to describe the excitonic dynamics. τ_{rise}, defined as the time elapsed from the excitation until the luminescence reaches a maximum, characterizes the time that the excitons need to reach the states from where they recombine after the unbound electrons and holes are created. τ_{dec} is obtained from an exponential fit of the temporal decay and reflects the mean lifetime of the excitons which give rise to light emission. Thus, the fast rise (∼5 ps) indicates that, with increasing excitation power, the creation of excitons responsible for the light emission is accelerated due to exciton–exciton interaction. On the other hand, the increase of τ_{dec} with power is caused by two factors: a saturation of the occupation of localized excitons and heating of an important number of excitons due to elastic exciton–exciton scattering.

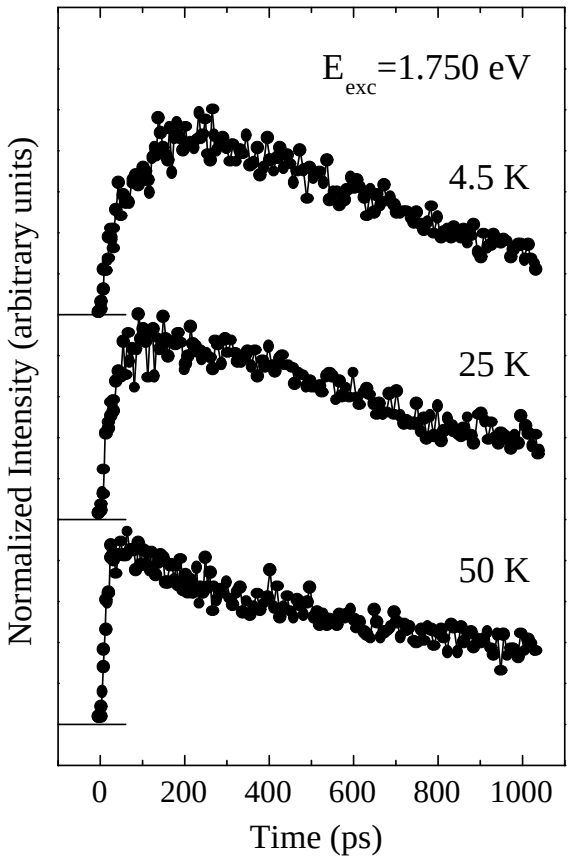

Figure 3. Time evolutions of the PL emitted by the 120 Å $GaAs_{0.92}P_{0.08}$ QW at different temperatures, exciting at 1.750 eV with 10 mW.

The lattice T influences markedly the exciton dynamics. Figure 3(a) shows that τ_{rise} diminishes while τ_{dec} stays constant as T rises. The latter fact is compatible with the localized character of the excitons, which are not characterized by a well defined wavevector $\boldsymbol{K}$, thus the momentum does not need to be conserved in the radiative recombination. This is in contrast with the situation found for free excitons, which present an increase of τ_{dec} with increasing T [14, 15]. The decrease of τ_{rise} with increasing T evidences that the excitons become localized only after they have reached a thermal equilibrium with the lattice. This is expected, since a high exciton T is incompatible with

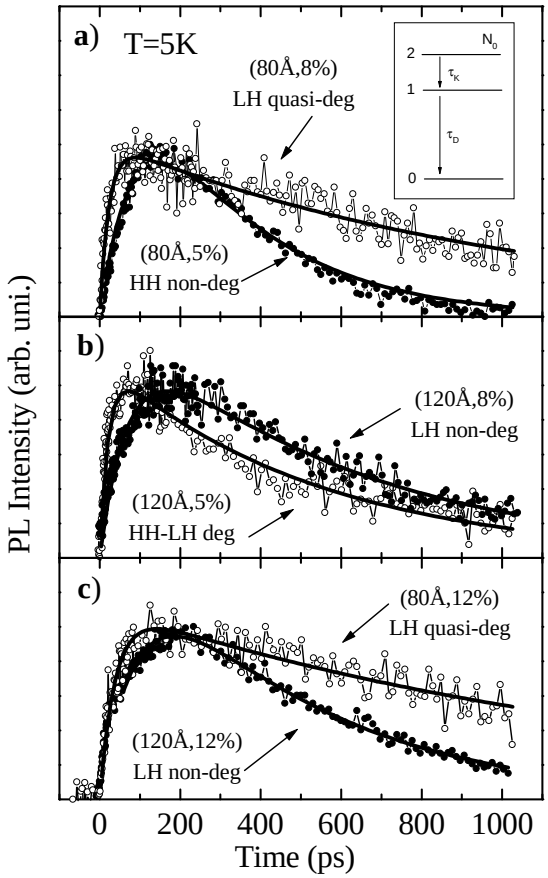

Figure 4. Low temperature time evolutions of the PL, emitted by the (80 Å, 8%) and (80 Å, 5%) QWs (a), (120 Å, 8%) and (120 Å, 5%) QWs (b) and (80 Å, 12%) and (120 Å, 12%) QWs (c). The intensity has been normalized to its maximum value. The lines are the best fits to the dynamic model shown in the inset figure.

localization. Furthermore, if the excitons became localized in an early stage no lattice-T dependence should be present since the bound excitons do not thermalize [16]. For free excitons, under our excitation conditions, the T of their initial thermal distribution is higher than that of the lattice. Then, if the lattice T is increased, the free excitons reach the equilibrium with the lattice in a shorter time, which is reflected in a reduction of τ_{rise}. This effect is similar and complementary to that observed in previous measurements where the lattice T was kept fixed and the excess energy of the excitation light was varied [17].

To study the influence of the band structure on the exciton dynamics, T will be kept at 5 K and the excitation density to the lowest possible value for each well. Under these conditions, we can minimize the saturation effects and the exciton–exciton scattering. The PL temporal evolutions will be fitted to a simple three level dynamic model shown in the inset of figure 4. At $t = 0$ there are N_0 electron–hole pairs in level 2. The transition $2 \rightarrow 1$ represents the relaxation to the localized states from where the excitons recombine, characterized by a time τ_K, and the transition $1 \rightarrow 0$ corresponds to the exciton recombination, characterized by the time τ_D. The dynamic equations which describe this model are:

$$\frac{\mathrm{d}N_2}{\mathrm{d}t} = -\frac{1}{\tau_K}N_2$$

$$\frac{\mathrm{d}N_1}{\mathrm{d}t} = -\frac{1}{\tau_D}N_1 + \frac{1}{\tau_K}N_2 \qquad \frac{\mathrm{d}N_0}{\mathrm{d}t} = +\frac{1}{\tau_D}N_1 \qquad (1)$$

and the initial conditions:

$$N_1(0) = N_0(0) = 0 \qquad \text{and} \qquad N_2(0) = N_0. \qquad (2)$$

The resolution of the system (1) with the initial conditions (2), taking into account that the temporal evolution of the PL intensity $I(t)$ is equal to $\mathrm{d}N_0/\mathrm{d}t$, leads to the following expression for $I(t)$:

$$I(t) = \frac{N_0}{\tau_K\tau_D((1/\tau_D) - (1/\tau_K))} \times(\exp(-t/\tau_K) - \exp(-t/\tau_D)). \qquad (3)$$

Figure 4 shows the temporal evolution of the luminescence emitted by the six investigated QWs. The lines are the best fits to the expression (3).

The times τ_K and τ_D obtained for each well are compiled in table 2. Some general features associated with the band structure of each well can be appreciated: (a) the wells with a degenerate or quasi-degenerate ground state show $\tau_K \sim 25$ ps; this value increases to $\tau_K \sim 90$ ps for non-degenerate wells. (b) The QW with an HH ground state shows $\tau_D \sim 300$ ps and those with an LH ground state $\tau_D \sim 500$ ps. (c) The (80 Å, 8%) and (80 Å, 12%) QWs present a specially large decay time, $\tau_D \sim 1$ ns.

The model we have employed is extremely simple, nevertheless, the good agreement of the fits with the experimental data indicates that two fundamental stages dominate the dynamic behaviour. The first stage is the exciton cooling, as can be inferred from the dependence of τ_K on the band structure. For low excitation densities, the cooling process occurs mainly by acoustic phonon interaction [3, 18, 19]. Since the probability of phonon interaction is proportional to the final density of states, the exciton cooling is faster in QWs with a degenerate ground state because the density of states is larger than that of the non-degenerate QWs. This is why the (120 Å, 5%), (80 Å, 8%) and (80 Å, 12%) QWs present a shorter τ_K, ∼25 ps, than the (80 Å, 5%), (120 Å, 8%) and (120 Å, 12%) QWs, ∼90 ps.

The second fundamental stage is the exciton recombination, which can happen either radiatively or non-radiatively. Only the radiative processes will reflect the effects of the band structure on τ_D. For two of the QWs, (80 Å, 8%) and (80 Å, 12%), we have found especially large values of $\tau_D \sim 1$ ns. These samples, with the narrowest wells and highest phosphorus content, are those less bright and with larger linewidths in the cw measurements. Therefore in the time-resolved measurements it was necessary to use relatively high excitation powers ($\geqslant$25 mW), which give rise to longer decay times, due to the saturation of the localized excitons as shown in figure 2. No correlation with the band structure could be drawn for these two samples. However, for the rest of the QWs, for which lower (∼5 mW) excitation powers could be employed, a clear dependence of τ_D on the heavy versus light character of the ground state has been obtained. The smaller value of τ_D for the QWs with an hh ground state is in agreement with the larger value of its oscillator strength as compared with that of the lh states [20].

Table 2. Characteristic exciton cooling (τ_K) and recombination (τ_D) times. They are obtained by fitting the time evolutions of the PL shown in figure 4, to the three level model of the inset of figure 4.

	(80 Å, 5%)	(120 Å, 5%)	(80 Å, 8%)	(120 Å, 8%)	(80 Å, 12%)	(120 Å, 12%)
τ_K (ps)	90 ± 5	21 ± 5	23 ± 5	70 ± 5	38 ± 5	93 ± 5
τ_D (ps)	277 ± 11	534 ± 18	1039 ± 46	590 ± 20	1389 ± 89	446 ± 12

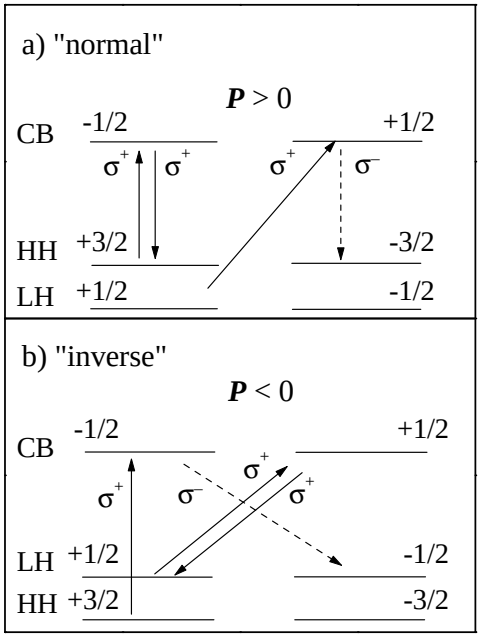

Figure 5. Spin levels of the conduction band (CB) and the hh (HH) and lh (LH) subbands. The arrows indicate the allowed transitions for the σ^+ and σ^- polarized light: (a) 'normal' configuration (the hh subband below the lh subband); (b) ' inverse' configuration (the lh subband below the hh subband). The polarization degree of the luminescence, $\boldsymbol{P}$, is positive in case (a) and negative in case (b).

3.2. The valence band mixing

The electronic band structure of a III–V semiconductor QW can be calculated using different approximations. The 'tight-binding' [21] or the 'pseudopotential' [22] methods provide a global description over the whole first Brillouin zone. A simpler approximation known as the 'envelope function formalism' (EFA) [23] provides a local description around any high symmetry point. The results obtained by any of these methods show that, while the dispersion relation of the CB is almost parabolic, the VB is strongly anisotropic. The hh and lh subbands are coupled, which implies that the third component of the angular momentum, m_J (which in this paper we will call the spin), is not a good quantum number. In other words, any electronic VB state has a certain probability of its spin being $+1/2$, $-1/2$, $+3/2$ or $-3/2$. This is usually known as the VBM.

We have analysed the influence of the electronic band structure on the degree of VBM, which could have important consequences on the hole spin relaxation time, as the VBM is the main mechanism responsible for the spin-flip of holes [6, 24]. We have used the empirical tight-binding method (TB) [25–27], which has been shown to be a valid alternative to EFA, since it improves the physical content in the description of the nanostructure with respect to $\boldsymbol{k}\cdot\boldsymbol{p}$ envelope function approaches without requiring a much higher computational effort. In particular, it allows us to treat indirect-gap semiconductors, heterostructures formed by indirect and direct materials, to describe very thin layers, etc [28–32]. We will only summarize here its main results.

3.2.1. The empirical tight-binding (TB) method. Optical properties can be obtained using the Kubo formula to define the susceptibility tensor, which is related to the current–current response function of the electromagnetic perturbation. This can be easily achieved within the tight-binding scheme *without* introducing new fitting parameters [33]. In a quantum well system and for a σ-polarized electromagnetic perturbation the squared optical matrix element can be written as [34, 35].

$$M^2_{cv}(\boldsymbol{k}_\parallel) = |\langle c, \boldsymbol{k}_\parallel|\boldsymbol{\sigma}\cdot\boldsymbol{J}|v, \boldsymbol{k}_\parallel\rangle|^2. \tag{4}$$

Here, $\boldsymbol{J}$ is the current operator, $\boldsymbol{\sigma}$ the polarization vector, c (v) label the conduction (valence) subbands including spin indexes, and $|n, \boldsymbol{k}_\parallel\rangle$ is the wavefunction for the nth subband with a given $\boldsymbol{k}_\parallel$ wave vector. The matrix elements of the current operator can be expressed in terms of the tight-binding matrix elements. Further details can be found elsewhere [34, 35].

For a given excitation energy (E) we calculate the excitation probability for the σ^+ polarization

$$P^+_x(c, v, E) = \int \mathrm{d}\boldsymbol{k}_\parallel |\langle c, \boldsymbol{k}_\parallel|\boldsymbol{\sigma}^+\cdot\boldsymbol{J}|v, \boldsymbol{k}_\parallel\rangle|^2 \times\delta(E - E_c(\boldsymbol{k}_\parallel) - E_v(\boldsymbol{k}_\parallel)) \tag{5}$$

where $E_n(\boldsymbol{k}_\parallel)$ is the nth subband dispersion.

The recombination probability is calculated considering that all the electrons are relaxed to $\boldsymbol{k}_\parallel = 0$

$$P^+_r(c, v) = |\langle c, \boldsymbol{0}|\boldsymbol{\sigma}^+\cdot\boldsymbol{J}|v, \boldsymbol{0}\rangle|^2 \tag{6}$$

$$P^-_r(c, v) = |\langle c, \boldsymbol{0}|\boldsymbol{\sigma}^-\cdot\boldsymbol{J}|v, \boldsymbol{0}\rangle|^2. \tag{7}$$

The luminescence intensity for each polarization and for an excitation energy E is given by

$$I^+(E) = \sum_{c,v,v'} P^+_x(c, v, E)P^+_r(c, v') \tag{8}$$

$$I^-(E) = \sum_{c,v,v'} P^+_x(c, v, E)P^-_r(c, v'). \tag{9}$$

In our calculation the excitation process involves the first two valence subbands and the first conduction subband, while the recombination process occurs between the first conduction subband and the first valence subband.

Finally the degree of polarization of the luminescence is calculated as:

$$P(t = 0, E) = (I^+(E) - I^-(E))/(I^+(E) + I^-(E)). \tag{10}$$

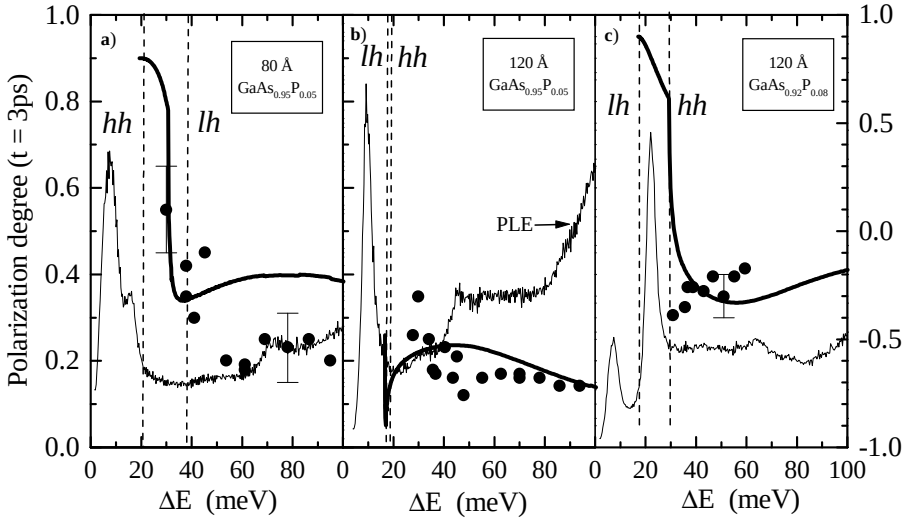

Figure 6. The solid points indicate the polarization degree of the luminescence at $t = 3$ ps as a function of the excess excitation energy, $\Delta E = E_{exc} - E_{det}$, for (a) the (80 Å, 5%) QW, whose band structure presents a 'normal' configuration, (b) the (120 Å, 5%) QW, whose band structure shows a 'degenerate' configuration and (c) the (120 Å, 8%) whose band structure reflects an 'inverse' configuration. The thick solid lines show the results of the tight-binding calculation. The vertical lines indicate the onset of the hh and lh subbands. The thin lines correspond to the PLE spectra.

For comparison with experiments, the calculated value of $\boldsymbol{P}(t = 0)$ has to be reduced to $\boldsymbol{P}(t_0)$, where $t_0 = 3$ ps is the half-width of the laser pulse; for this purpose, it has been considered that $P(t)$ decays exponentially with a characteristic time of 30 ps, as obtained from experiments. To mimic the effects of excitonic localization we have also included several $\boldsymbol{k}$ points for each transition; however the changes were not significant as compared to the single $\boldsymbol{k}$ calculations therefore only these latter results will presented. In the present work we use a relativistic-sp^3s^* tight binding where the parameters are obtained by using the virtual crystal approximation on the GaAs [30], AlAs [30] and GaP [36] parametrizations.

3.2.2. Experimental study. The excitation with circularly polarized light allows the selection of the spin of the photoexcited carriers because the population of the excited electrons and holes with a certain spin depends on the excitation energy, E_{exc}. If we assume that the spin relaxation of holes is very fast [37], ∼4 ps, the intensity of the $\sigma^+(\sigma^-)$ polarized light, $I^+(I^-)$, at short times, before the electron spin relaxation takes place, will reflect the initial population of photoexcited electrons with a certain spin. Thus, the study of the polarization degree of the PL at $t = 0$, $\boldsymbol{P}(0) = (I^+(0) - I^-(0))/(I^+(0) + I^-(0))$, as a function of E_{exc}, will give relevant information about the dependence of the VBM on $\boldsymbol{k}$.

Figure 5 shows schematically the allowed transitions between the VB and the CB when the system is excited (↑ arrows) by σ^+ polarized light. The emission (↓ arrows) is limited to the lowest level of the VB. Case (a) corresponds to a well with a 'normal' configuration (hh subband below the lh one in the growth direction) and case (b) to a well with an 'inverse' configuration†. For the sake of clarity, let us begin considering the situation with no VBM. In both cases, (a) and (b), the excitation of only the lower subband will give rise to $\boldsymbol{P}(0) = 1$:

$$\boldsymbol{P}(0) = \frac{1-0}{1+0} = 1. \tag{11}$$

When both subbands are excited, taking into account that the oscillator strength of the hh transitions is three times stronger than that of the lh transitions, $\boldsymbol{P}(0)$ must ideally be +0.5 for case (a) and −0.5 for case (b): $\boldsymbol{P}(0) = (0.75 - 0.25)/(0.75 + 0.25) = +0.5$, in the 'normal' and $\boldsymbol{P}(0) = (0.25 - 0.75)/(0.25 + 0.75) = -0.5$ for the 'inverse' case. Any deviation of $|\boldsymbol{P}(0)|$ from 0.5 is due to the VBM effects and $|\boldsymbol{P}(0)|$ becomes lower than 0.5.

3.2.3. The band-structure dependence. The only $GaAs_{1-x}P_x$ QW with a 'normal' configuration, i.e., with the hh subband below the lh one, and with an HH ground state is the (80 Å, 5%) QW. Figure 6(a) shows $\boldsymbol{P}(t_0)$ as a function of the difference between the excitation and detection energies, $\Delta E = E_{exc} - E_{det}$. The solid points correspond to the experimental results. The thin line depicts the PLE spectrum. The zero of ΔE is set at the energy which corresponds to the maximum of the PL spectrum. The two vertical lines indicate the onsets of the hh and lh subbands. The TB calculation is indicated by a thick continuous line. Our experimental setup and the low intensity of the luminescence limits the lowest value of ΔE to ∼30 meV. At this energy, $\boldsymbol{P}(t_0)$ is 0.55. For excitation above the lh subband, a clear decrease of $\boldsymbol{P}(t_0)$ up to ∼0.25 is observed. This is in qualitative agreement with the calculation, which shows a large decay of $\boldsymbol{P}(t_0)$ from ∼0.94, below the lh subband, down to 0.4 for $\Delta E > 40$ meV. The difference from the ideal value of 0.5 reflects the VBM. The discrepancy between theory and experiments above the lh subband edge could be due to excitonic effects and localization of excitons which has not been taken into account in the calculation. The localization

† In figure 5, the levels denoted by HH and LH must be understood as discrete excitonic levels in emission and as the electronic continuum in absorption.

produces a partial violation of the $\boldsymbol{K}$-conserving rule [38], which allows the recombination of excitons with $\boldsymbol{K} \neq 0$.

Figure 6(b) shows the results for the (120 Å, 5%) QW, which has an HH–LH degenerate ground state. In spite of the negative value of Δ, as illustrated by the two vertical lines, $\boldsymbol{P}(t_0)$ takes positive values. This is due to the proximity of the HH and LH excitonic peaks: the PL originates from the radiative recombination of both types of exciton. As the oscillator strength of the $\pm 3/2$ transitions is three times larger than that of the $\pm 1/2$ transitions [20], the intensity of the emission due to the +1 excitons dominates that of the -1 excitons. Figure 6(b) reflects a strong VBM for $\Delta E > 40$ meV since $\boldsymbol{P}(t_0)$ becomes as low as 0.15. Again, the experimental results are in good agreement with the theory, which predicts a polarization degree of $\sim$0.2–0.15 above the hh–lh subband edges.

The results for the (120 Å, 8%) QW, which has an 'inverse' configuration, are shown in figure 6(c). The two peaks of the PLE spectrum at $\Delta E = 7$ meV and $\Delta E = 22$ meV correspond to LH and HH, respectively. It is interesting to note that exciting above the hh subband edge, $\boldsymbol{P}(t_0)$ takes negative values, as indicated in the scheme of figure 5. The TB calculations predict a strong VBM in the spectral range between the lh and hh subbands. Unfortunately, we can not access these energies experimentally. For excitation above the hh subband, the calculated $\boldsymbol{P}(t_0)$ is in good agreement with the experimental results.

The degree of VBM, which is reflected by the difference between $|\pm 0.5|$ and the obtained values of $|\boldsymbol{P}(t_0)|$, of the QWs shown in figure 6(a) and figure 6(c) is similar: $|\boldsymbol{P}(t_0)|$ is $\sim$0.3 for both QWs which means a reduction of 40% in relation to the value of $\boldsymbol{P}(t_0)$ in the absence of VBM, $|\pm 0.5|$. As figure 6(b) shows, *the VBM is stronger in QWs with a degenerate ground state*. In (120 Å, 5%) and (80 Å, 12%) QWs, $|\boldsymbol{P}(t_0)|$ becomes lower than 0.2, which indicates a reduction of 70%. This reflects a higher coupling between the hh and lh subbands. In [9], it was shown that the effective masses of the hh and lh subbands in the degenerate QWs are larger than those of the non-degenerate QWs, and this was interpreted as a consequence of the stronger coupling between the bands. This is also borne out in our present experiments, which show that the VBM is larger in the degenerate case. This enhancement of the VBM in the degenerate cases could have important consequences for the spin relaxation time of holes. The hole depolarization occurs simultaneously with the momentum relaxation, since the degree of VBM (and thus the spin mixing) depends on $\boldsymbol{k}$. The increment of the VBM in the degenerate cases could shorten the hole spin relaxation time below 4 ps, the shortest hole depolarization time observed [37] to our knowledge.

4. Summary

Exciton cooling dominates the excitonic dynamics in $GaAs_{1-x}P_x$ QWs. It is faster in QWs with an HH–LH degenerate excitonic ground state than in non-degenerate QWs. The coincidence of both bands at the Γ point increases the final density of states for the scattering of excitons by acoustic phonons. For the QWs with this type of excitonic configuration, the cooling occurs only in $\sim$25 ps, whereas for the QWs with a non-degenerate excitonic ground state, the time increases to $\sim$90 ps. The exciton recombination time is determined by the hh or lh character of the ground state. If this is HH, the time is $\sim$300 ps, whereas if it is LH, it increases up to $\sim$500 ps. This is in agreement with the larger oscillator strength of the HHs compared to that of the LHs.

Moreover, we have observed an important increment of the valence band mixing in structures where hh and lh subbands are very close. In these degenerate cases, the valence band mixing reduces the initial degree of the polarization by 70%, while in systems with a non-degenerate configuration the reduction diminishes to 40%. The experimental results are in qualitative agreement with valence band mixing calculations based on the empirical tight-binding model.

Acknowledgments

This work was partially supported by 'Fundación Ramón Areces', the Spanish DGICYT under contract PB96-0085 and European Union Network FMRX-CT970134.

References

[1] Singh J 1991 *Condensed Systems of Low Dimensionality* (New York: Plenum)
[2] O'Reilly E P 1989 *Semicond. Sci. Technol.* **4** 121
[3] Damen T C *et al* 1990 *Phys. Rev.* B **42** 7434
[4] Kothiyal G P *et al* 1987 *Appl. Phys. Lett.* **51** 1091
[5] Hong S *et al* 1988 *Phys. Rev.* B **37** 878
[6] Ferreira R and Bastard G 1991 *Phys. Rev.* B **43** 9687
[7] Bertolet D C, Hsu J and Lau K M 1988 *Appl. Phys. Lett.* **53** 2501
[8] Koteles E S *et al* 1990 *Surf. Sci.* **228** 314
[9] Viña L *et al* 1993 *Phys. Rev.* B **47** 3926
[10] From now on, (L_z Å, x%) denotes a QW whose well width is L_z Å and whose phosphorus composition is x%.
[11] Bastard G *et al* 1984 *Phys. Rev.* B **29** 7042
[12] Vinattieri A *et al* 1994 *Phys. Rev.* B **50** 10 868
[13] Shah J 1996 *Ultrafast Spectroscopy of Semiconductors and Semiconductor Nanostructures* (Heidelberg: Springer)
[14] Feldmann J *et al* 1987 *Phys. Rev. Lett.* **59** 2337
[15] Colocci M, Gurioli M and Martinez-Pastor J 1993 *J. Physique Coll.* IV **3** C5 3
[16] Gurioli M, Vinattieri A, Martinez-Pastor J and Colocci M 1994 *Phys. Rev.* B **50** 11 817
[17] Eccleston R *et al* 1991 *Phys. Rev.* B **44** 1395
[18] Leo K, Rühle W W, Queisser H J and Ploog K 1988 *Phys. Rev.* B **37** 7121
[19] Ryan J F and Tatham M 1989 *Solid State Electron.* **32** 1429
[20] Pollak F H and Cardona M 1968 *Phys. Rev.* **172** 816
[21] Chang Y-C and Schulman J N 1982 *J. Vac. Sci. Technol.* **21** 540
[22] Jaros M, Wong K B and Gell M A 1985 *Phys. Rev.* B **31** 1205
[23] Bastard G 1990 *Wave Mechanics Applied to Semiconductor Heterostructures* (Les Ulis: Éditions de Physique)
[24] Uenoyama T and Sham L J 1990 *Phys. Rev.* B **42** 7114
[25] Slater J C and Koster G F 1954 *Phys. Rev.* **94** 1498
[26] Bullet D W 1980 *Solid State Physics* vol 35 (New York: Academic) p 129
[27] Majewski J A and Vogl P 1989 *The Structure of Binary Compounds* ed F R de Boer and D G Pettifor (Amsterdam: Elsevier) p 287
[28] Boykin T B, van der Wagt J P A and Harris J S 1991 *Phys. Rev.* **43** 4777
[29] Di Carlo A and Lugli P 1995 *Semicond. Sci. Technol.* **10** 1673

[30] Schulman J N and Chang Y C 1985 *Phys. Rev.* B **31** 2056
[31] Zunger A, Yeh C-H, Wang L-W and Zang S B 1995 *22nd Int. Conf. on Physics of Semicondictors* ed D J Lockwood (Singapore: World Scientific) p 1763
[32] Di Carlo A, Reale A, Tocca L and Lugli P 1998 *IEEE J. Quantum Electron.* **34** 1730
[33] Graf M and Vogl P 1995 *Phys. Rev.* **51** 4940
[34] Di Carlo A *et al* 1996 *Solid State Commun.* **98** 803
[35] Di Carlo A 1998 *Tight-Binding Approach to Computational Materials Science (Mater. Res. Soc. Symp. Proc. 491)* (Pittsburgh, PA: Materials Research Society) p 389
[36] Priester C, Allan G and Lannoo M 1988 *Phys. Rev.* B **37** 8519
[37] Damen T C *et al* 1991 *Phys. Rev. Lett.* **67** 3432
[38] Schnabel R F *et al* 1992 *Phys. Rev.* B **46** 9873